Bioorganic Chemistry 89 (2019) 103025

Contents lists available at ScienceDirect

Bioorganic Chemistry

journal homepage: www.elsevier.com/locate/bioorg

Design and development of 1,3,4-oxadiazole derivatives as potential inhibitors of acetylcholinesterase to ameliorate scopolamine-induced cognitive dysfunctions

Puja Mishra, Piyoosh Sharma, Prabhash Nath Tripathi, Sukesh Kumar Gupta, Pavan Srivastava, Ankit Seth, Avanish Tripathi, Sairam Krishnamurthy, Sushant Kumar Shrivastava*

Department of Pharmaceutical Engineering & Technology, Indian Institute of Technology (Banaras Hindu University), Varanasi 221 005, India

ARTICLE INFO

Keywords:
Acetylcholinesterase
Butyrylcholinesterase
1,3,4-Oxadiazole
Molecular hybridization
4-Aminopyridine

ABSTRACT

The novel hybrids bearing 4-aminopyridine (4-AP) tethered with substituted 1,3,4-oxadiazole nucleus were designed, synthesized, and evaluated for their potential AChE inhibitory property along with significant antioxidant potential. The inhibitory potential (IC_{50}) of synthesized analogs was evaluated against human cholinesterases (hAChE and hBChE) using Ellman's method. Among all the compounds, **9** with 4-hydroxyl substituent showed maximum hAChE inhibition with the non-competitive type of enzyme inhibition (IC_{50} = 1.098 μM; Ki = 0.960 μM). Further, parallel artificial membrane permeation assay (PAMPA-BBB) showed significant BBB permeability in most of the synthesized compounds. Meanwhile, compound **9** also inhibited AChE-induced Aβ aggregation (38.2–65.9%) by thioflavin T assay. The *in vivo* behavioral studies showed dose-dependent improvement in learning and memory by compound **9**. The *ex vivo* studies also affirmed the significant AChE inhibition and antioxidant potential of compound **9** in brain homogenates.

1. Introduction

Severity and prevalence of neurocognitive disorders especially dementia with shocking, demoralizing, and life-threatening consequences on the life of patients represents a substantial challenge for the scientific community [1]. The manifestations of decline in cognitive functions are reported in several neurodegenerative disorders like schizophrenia, Alzheimer's disease (AD), traumatic brain injury, Parkinson's disease, etc. [2]. AD is one of the major neurocognitive disorders and a prominent cause of death in the elderly population worldwide [3]. The recently published World Alzheimer's report 2018 has emphasized to explore new dimensions for the treatment and increase the research expenditure for the new drug discovery as the number of dementia patients are increasing day by day [4,5].

The two widely explored therapeutic strategies for the AD are declined cholinergic transmission and amyloid beta aggregation [6,7]. Acetylcholinesterase (AChE) is a serine hydrolase enzyme responsible for the hydrolysis of ACh, thereby reducing the levels of ACh which was reported to be in close association with cognitive decline [8–12]. The preceding several years have witnessed the discovery of numerous AChE inhibitors that concreted the way for a superior therapeutic strategy towards cognition enhancement associated with AD [13–16]. However, the currently available pharmacotherapies are failed to address all the pathogenic hallmarks of the disease and unable to sojourn the disease progression [17,18]. AChE has also been recognized to play a vital role in increasing the deposition of Aβ aggregates in AD [19]. The aggregation and deposition of Aβ fibrils and oligomers leads to disruption of cellular communication, inflammatory responses, progressive neuritic injury, neuronal deficits, and cognitive dysfunctions [5,20]. Accumulation of Aβ could also lead to oxidative damage in the brain by entering into mitochondria and increasing generation of free radicals [21].

The synthetic versatility and broad spectrum of therapeutic potentials of oxadiazole have been the center of attraction to pharmaceutical scientists in last few decades. Unique structural features of oxadiazole lead to the discovery of some structurally diverse derivatives with reported inhibitory activity against AChE as well as amyloid beta [22–24]. 4-Aminopyridine (4-AP) is another heterocyclic nucleus reported for antiamnesic activity, cognition enhancement and inhibition of AChE [14,25,26]. The accumulating lines of evidence suggested that hybridization of two or more diverse bioactive molecules with corresponding pharmacophoric functions or with different mechanisms of

* Corresponding author.
E-mail address: skshrivastava.phe@itbhu.ac.in (S.K. Shrivastava).

https://doi.org/10.1016/j.bioorg.2019.103025
Received 8 February 2019; Received in revised form 13 April 2019; Accepted 30 May 2019
Available online 31 May 2019

action render synergistic effects contributing to the overall activity profile of the molecule [27,28]. In the current research, a novel series of compounds were designed and synthesized by invoking the concept of molecular hybridization. The synthesized compounds were evaluated for their *in vitro* potential against AChE and butyrylcholinesterase (BChE) along with the assessment of their permeability across the blood–brain barrier (BBB) by parallel artificial membrane permeability assay (PAMPA-BBB) and AChE-induced amyloid beta aggregation inhibitory potential. The outcomes of *in vitro* results were further corroborated using *in vivo*, *ex* vivo and *in silico studies*.

1.1. Designing considerations

In our previous research work, we have reported 4-AP based semicarbazones (**I**), Schiff bases (**II**), and other derivatives (**III** and **IV**) for their potential antiamnesic and cognition-enhancing properties with significant cholinesterase inhibition profile [13,14,26]. The 4-AP nucleus itself was examined by dose-finding studies in the patients of the AD, but no significant effect was observed due to the unselective release of neurotransmitters and poor penetrability of 4-AP in CNS [29]. These studies have prompted us to select the 4-AP pharmacophoric core group to design novel hybrids.

The oxadiazole nucleus reported to possess diverse pharmacological activities such as anti-microbial [30], antimalarial [31], anticancer [32], antidepressant [33], antifungal [34], antiviral [35], anti-inflammatory [28], analgesic [36], muscle relaxants [37] etc. Also, the versatile nature of the 1,3,4-oxadiazole scaffold with varied substitution (**V**, **VI**, and **VII**) has been reported for significant anti-cholinesterase and antioxidant activities [38,39]. At 2nd position of 1,3,4-oxadiazole nucleus, 4-AP pharmacophoric core group was linked, and the remaining 5th position was connected with aryl group substituted with variable electron withdrawing and donating functional groups. Herein, we have designed the cyclized analogues of semicarbazones and bioisosterically replaced it with 1,3,4-oxadizole nucleus to impart gastric stability and improve its efficacy.

On the basis of above-mentioned conjectures, we have designed molecular hybrids of 4-AP tethered with a substituted 1,3,4-oxadiazole nucleus (Fig. 1). These molecular hybrids were designed as per the structural requisites for potential cholinesterase inhibitory activity with the hypothesis that 4-AP will extend into the catalytic site, and substituted 1,3,4-oxadiazole will efficiently interact with the peripheral anionic site residues of AChE similar to the piperidine nucleus and indanone ring of donepezil, respectively.

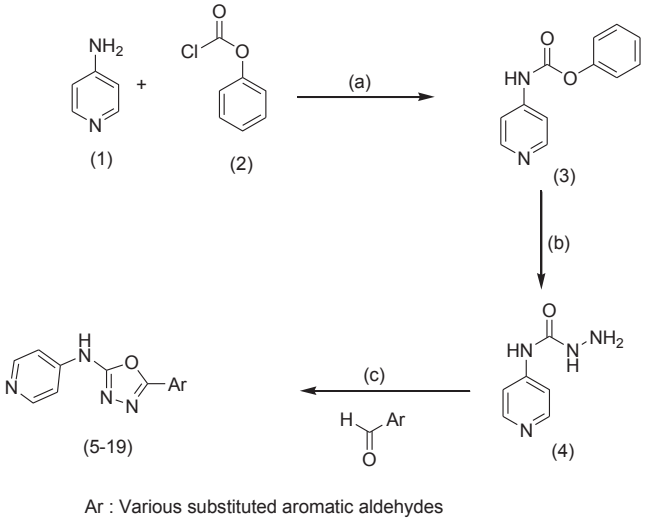

Scheme 1. Synthetic scheme: (a) Pyridine (2.3 eq), dichloromethane (15 ml), stirring 0–5 °C 8 h (b) hydrazine hydrate (3 eq), absolute ethanol, reflux 1 h; (c) substituted aldehydes (1 eq), glacial acetic acid (1–2 drops), absolute ethanol, reflux 3–5 h followed by addition of chloramine-T, stirring 2–3 h.

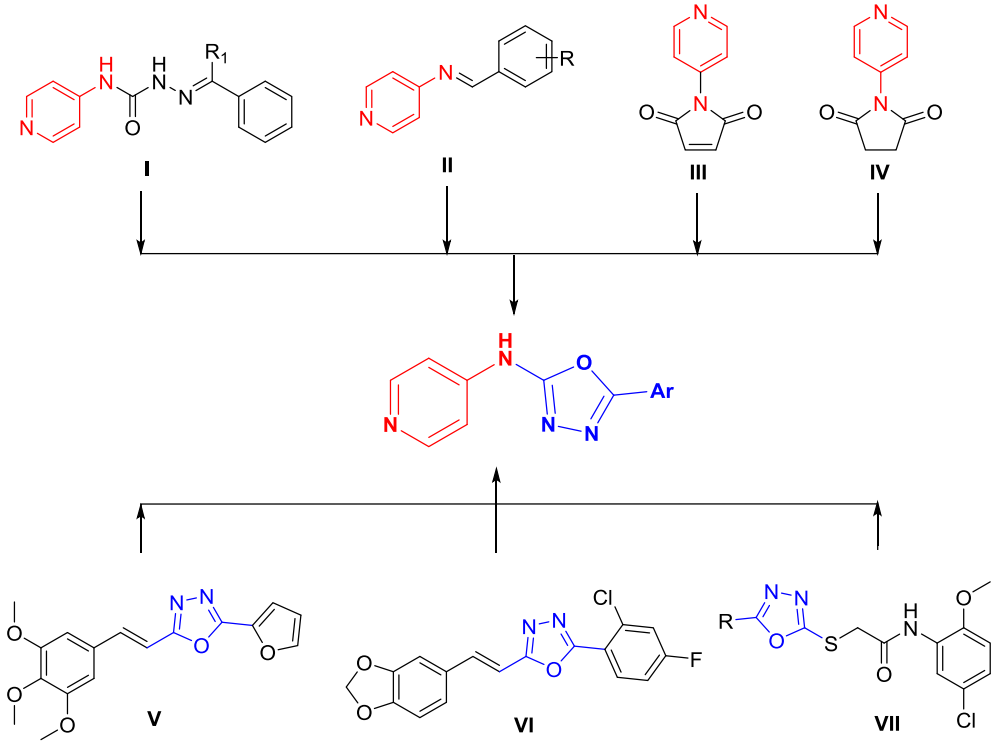

Fig. 1. Designing of 4-AP tethered substituted 1,3,4-oxadiazole analogs.

2. Results and discussion

2.1. Chemistry

The designed analogs (**5–19**) were synthesized following the procedure mentioned in Scheme 1. The 4-AP (**1**) was reacted with phenyl chloroformate to acquire the intermediate (**3**) and used further without purification. Intermediate (**3**) was reacted with an excess of hydrazine hydrate to get the key intermediate (**4**). In the final step, various aromatic aldehydes and intermediate (**4**) were refluxed for 3–5 h to afford respective semicarbazones, which were *in situ* proceeded with chloramine-T for cyclization to afford the target compounds (**5–19**).

The FT-IR spectra exhibited the characteristic secondary amine (−NH) stretching in the range 3496–3191 cm^{-1} to confirm the cyclization of the Schiff bases into oxadiazole ring. In the ^{1}H NMR spectral analysis, formation N=CH bonds were characterized by the presence of a peak between δ_H 8.71–8.23 ppm. The disappearance of the $-NH_2$ of compound **4** and appearance of the −NH peak of 1,3,4-oxadiazole derivatives that occurs variably around δ_H 9.21–8.10 ppm confirmed the cyclization. Two aromatic groups were confirmed by ^{13}C NMR showing the peaks in the range of δ_C 155–104 ppm. Compound (**9**) having the carbon attached to hydroxyl group showed the peak in the downfield region at δ_C 167 ppm. The derivatives have a substitution at 2nd and 5th position of a 1,3,4-oxadiazole heterocyclic moiety having pyridine ring on one end and substituted aromatic ring on the other end were also characterized by elemental (C, H, and N) analyses and the results were found within the range of theoretical limits (± 0.4%). The results of physicochemical characterization are given in Table 1.

2.2. Pharmacology

2.2.1. Cholinesterase inhibition assay

Ellman colorimetric assay was used to determine the inhibition property of compounds **5–19** against AChE and BChE using donepezil as positive reference standard [40]. The results of IC_{50} values against AChE and BChE mentioned in Table 2 indicated the micromolar inhibition of AChE by most of the compounds. The unsubstituted aryl ring in compound **5**, p-substituted compounds (**7**, **9**, **12**, **14**, and **18**), and trimethoxy substituted compound **19** showed micromolar inhibitory potential against AChE. Among the tested compounds, compound **9** with p-hydroxy substituent showed maximum inhibitory potential against AChE (IC_{50} = 1.098 ± 0.140 μM). The compound **9** also showed maximum selectivity for AChE inhibition as compared to other tested derivatives. Interestingly, 3-tolyl substituted derivative showed better BChE inhibitory potential than AChE. Among other p-substituted derivatives, only compounds **7**, **9**, **12**, and **14** have demonstrated micromolar inhibitory potency against BChE in the IC_{50} range of 7.794–9.220 μM. The compound **9** also exhibited the maximum selectivity index for AChE over BChE compared to other tested derivatives.

Table 1
Structural hybrids of synthesized 4-AP tethered 1,3,4-oxadiazole analogs and results of their physicochemical characterization.

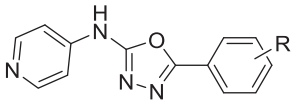

(5-19)

Compound	R-group	R_f*	Melting point (°C)	LogP**
5	−H	0.37	207–209	2.48
6	3−Br	0.42	211–213	3.31
7	4−Br	0.43	241–243	3.38
8	2−OH	0.30	188–190	2.02
9	4−OH	0.28	198–200	2.18
10	2−NO_2	0.41	215–217	2.32
11	3−NO_2	0.42	230–232	2.40
12	4−NO_2	0.36	232–234	2.45
13	3−Cl	0.38	218–220	3.18
14	4−Cl	0.46	227–229	3.30
15	2,3−diCl	0.52	246–248	3.68
16	3−CH_3	0.34	236–238	2.96
17	4−CH_3	0.35	245–247	3.08
18	4−OCH_3	0.38	223–225	2.38
19	3,4,5−triOCH_3	0.32	212–214	2.16

* Rf values were determined using dichloromethane:methanol (9.5:0.5 v/v) as the mobile phase.

** LogP values were determined by octanol:water-based shake flask test.

2.2.2. Enzyme kinetics

The mechanism of AChE inhibitory potential by compound **9** was investigated by enzyme kinetics study. The reciprocal Lineweaver-Burk plot showed inhibition of hAChE through a non-competitive mechanism in which the value of V_{max} decreased, and K_m remained constant (Ki = 0.960 μM) (Fig. 2). The intersection points on both axes of $1/V_{max}$ and 1/[S] were found to be higher than zero, suggesting that the inhibitor was preferentially bound to free enzyme rather than enzyme-substrate complex.

2.2.3. PAMPA-BBB assay

The essential requirement of the synthesized compounds is their permeability through the blood-brain barrier (BBB) to be efficacious in neurodegenerative disorder [41]. Therefore, permeability of compounds was evaluated by PAMPA-BBB assay. The permeability of compounds from donor microplate to acceptor microplate was most accurately determined through a porcine brain lipid layer. The permeability of nine commercial drugs as reported in our previously published report was used as a benchmark to establish the correlation between experimental $P_{e(exp)}$ and reference permeability $P_{e(ref)}$ [42]. The CNS permeability cut-off values indicated that compounds with permeability (P_e) over 4.3926×10^{-6} cm s^{-1} suggest excellent brain penetrability, whereas with $P_e < 1.7766 \times 10^{-6}$ cm s^{-1} has poor brain permeation. The permeability value in between them was considered as uncertain [43]. The results indicated that compounds **5, 6, 7, 9, 14, 17, 18,** and **19** showed excellent brain permeability. Compounds **8**, **10, 12, 13, 15,** and **16** showed moderate permeation characteristics. Only compound **11** among all the tested compounds showed very low CNS brain permeability (Table 2).

2.2.4. AChE-induced amyloid beta aggregation inhibition: Thioflavin T assay

The AChE was demonstrated to be involved in the promotion of Aβ aggregation by specifically binding to PAS [44,45]. The role of AChEIs has been validated to prevent the Aβ aggregation and deposition. Therefore, thioflavin T based fluorometric assay was performed for compound **9** to ascertain its role in inhibiting and preventing Aβ aggregation. The test was conducted at three different ratios of Aβ: compound **9** (10:5, 10:10, and 10:20 μM). The results were reported as % Aβ aggregation inhibition (Fig. 3A) and normalized fluorescence intensity (NFI) (Fig. 3B). The results indicated comparable anti-aggregatory property of compound **9** (38.2–65.9%) with donepezil (39.6–68.9%). The inhibitory potential increased with increasing concentration ratio of inhibitor.

2.2.5. In vivo behavioral studies

Compound **9** showed promising *in vitro* AChE inhibitory potential and high brain permeability through *in vitro* PAMPA-BBB assay. These results have prompted us to evaluate the compound **9** through *in vivo* behavioral models in animals. The scopolamine-induced models are very well validated models of learning and memory [46]. The

Table 2
The results of cholinesterase inhibitory potential and prediction of brain permeability of the synthesized compounds.

Comp. Code	R-group	IC_{50} μM ± SEM[a]		SI for hAChE[b]	PAMPA-BBB permeability[c] $P_{e(exp)}$ (10^{-6} cm s^{-1})	PAMPA-BBB Prediction (CNS + [d], CNS-[e], CNS ± [f])
		hAChE	hBChE			
5	−H	8.714 ± 0.255	> 10	–	5.39 ± 0.11	CNS +
6	3−Br	> 10	> 10	–	6.75 ± 0.07	CNS +
7	4−Br	2.535 ± 0.212	8.793 ± 0.474	3.47	7.02 ± 0.06	CNS +
8	2−OH	> 10	> 10	–	3.62 ± 0.34	CNS ±
9	4−OH	1.098 ± 0.140	7.794 ± 0.084	7.10	4.65 ± 0.21	CNS +
10	2−NO_2	> 10	> 10	–	3.41 ± 0.13	CNS ±
11	3−NO_2	> 10	> 10	–	1.56 ± 0.12	CNS-
12	4−NO_2	1.986 ± 0.155	7.351 ± 0.329	3.70	2.64 ± 0.18	CNS ±
13	3−Cl	> 10	> 10	–	3.36 ± 0.08	CNS ±
14	4−Cl	4.356 ± 0.235	9.220 ± 0.238	2.12	4.57 ± 0.11	CNS +
15	2,3−diCl	> 10	> 10	–	3.79 ± 0.03	CNS ±
16	3−CH_3	> 10	8.322 ± 0.231	–	3.20 ± 0.02	CNS ±
17	4−CH_3	6.173 ± 0.194	> 10	–	5.64 ± 0.35	CNS +
18	4−OCH_3	2.208 ± 0.233	> 10	–	4.65 ± 0.24	CNS +
19	3,4,5−triOCH_3	1.790 ± 0.074	7.472 ± 0.227	4.17	7.34 ± 0.14	CNS +
donepezil		0.043 ± 0.007	4.327 ± 0.459	100.63	nd	nd

nd = Not determined.
[a] All the results are reported as IC_{50} ± SEM (n = 3).
[b] SI (Selectivity Index) = (IC_{50} BChE)/(IC_{50} AChE).
[c] Data represented are the mean ± SEM of two independent experiments (n = 2).
[d] 'CNS +' (prediction of high BBB permeation); P_e (10^{-6} cm s^{-1}) > 4.3926.
[e] 'CNS −' (prediction of low BBB permeation); P_e (10^{-6} cm s^{-1}) < 1.7766.
[f] 'CNS ± ' (prediction of uncertain BBB permeation); P_e (10^{-6} cm s^{-1}) 4.3926 to 1.7766.

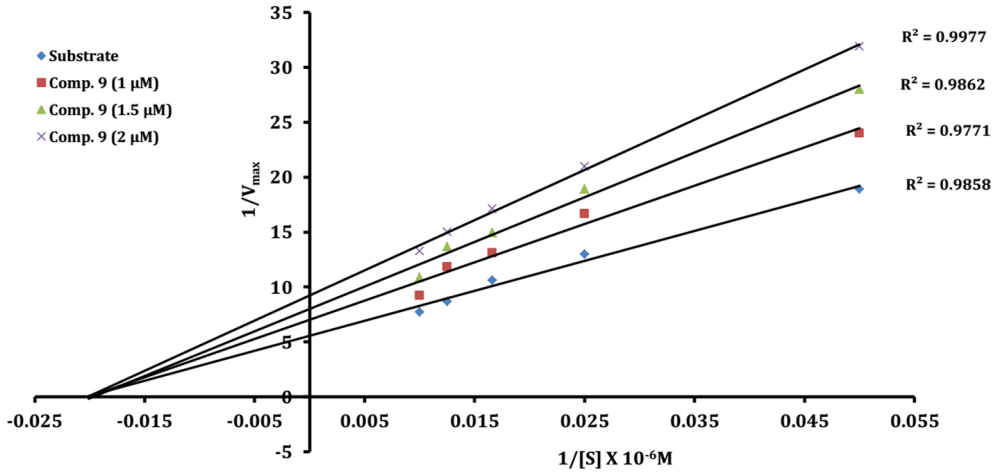

Fig. 2. Lineweaver-Burk plot showing non-competitive inhibition of compound 9.

antiamnesic effect of compound **9** was evaluated using the Y-maze and passive avoidance tests in mice.

2.2.5.1. Acute toxicity study. Acute toxicity of compound **9** was determined on healthy Swiss Albino mice (25–30 gm) as per the OECD 423 guidelines. Several behavioral, cholinergic effects, and toxic reactions were monitored such as tremors, convulsions, salivation, diarrhea, sleep, lacrimation, and feeding behavior. There were no signs of any cholinergic side effects, any toxicity, or no mortality was observed post administration of test compound **9**. These studies suggested that compound **9** have a significant margin of safety [42].

2.2.5.2. Y-maze test. The Y-maze test is the standard animal model used for evaluation of hippocampal-dependent short-term working memory in the rodents [47]. The percentage (%) alterations were calculated (spontaneous alteration rate), which demonstrated the working memory capacity of animals. The % spontaneous alternations was significantly reduced ($^{***}p < 0.001$) in the scopolamine group of animals compared to control group indicative of induction of memory and learning impairment. Donepezil (5 mg/kg) and compound **9** showed significantly increased ($^{\#\#\#}p < 0.001$) spontaneous alternations compared to scopolamine group. At the dose of 5 and 10 mg/kg, p.o. compound **9** showed statistically non-significant difference in % spontaneous alterations compared to donepezil (5 mg/kg) (Fig. 4A). The total arm entries remained unchanged in all groups suggested that scopolamine did not hamper the locomotor activity in animals (Fig. 4B).

2.2.5.3. Passive avoidance test. This model is primarily responsible for hippocampal and cholinergic neuronal dysfunctions [48]. Transfer latency time was calculated in seconds for the transfer of mice from the light chamber to the dark chamber. The increase in transfer latency (TL) period suggested the improvement in learning and memory in rodents. Scopolamine-induced amnesia leads to no significant change in the latency period between the acquisition phase and retention phase indicated the loss of learning and memory. But, the treatment with compound **9** showed significantly increased ($^{*}p < 0.05$) TL in a dose

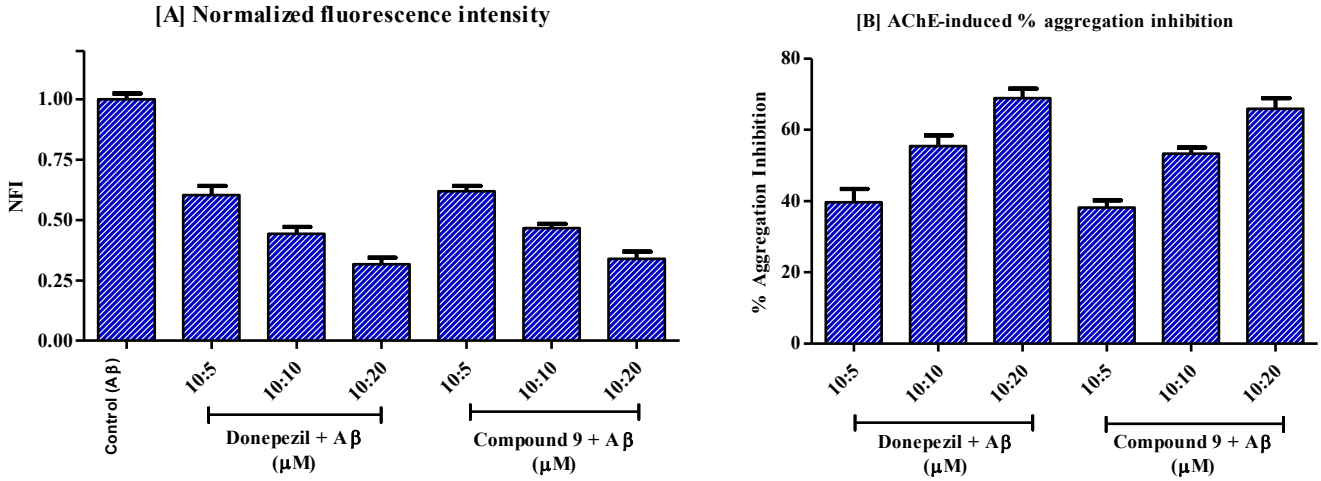

Fig. 3. Effect of compound **9** and donepezil in thioflavin T assay. [A] Normalized fluorescence intensity (NFI); [B] % aggregation inhibition. Each bar displays the mean ± SEM of three separate experiments (n = 3).

dependent manner compared to the scopolamine-treated group. Moreover, during retention test, results of compound **9** at the dose of 5 and 10 mg/kg showed non-significant difference with donepezil (Fig. 5). The overall results of scopolamine-induced models advocated the potential of compounds **9** in improving spatial and immediate working memory.

2.2.6. *Ex vivo* and biochemical analysis

The effect of compound **9** on brain AChE level was evaluated by *ex vivo* study as per Ellman's method [40]. The results showed a significantly higher rate (Fig. 6A, $^{***}p < 0.001$) of substrate hydrolysis or elevated levels of AChE in the scopolamine group of animals compared to control group. The levels of AChE were remarkably attenuated (Fig. 6A, $^{\#\#\#}p < 0.001$) by treatment of compound **9** in a dose dependent manner compared to the scopolamine group. The *ex vivo* brain AChE inhibitory potential of compound **9** at the dose of 10 mg/kg was found to be statistically non-significant in comparison to donepezil. These results also reflected the ability of compound **9** to permeate the BBB.

The antioxidant potential of compounds was elucidated by estimation of oxidative biochemical markers such as malonaldehyde (MDA, lipid peroxidation by-product), superoxide dismutase (SOD, involved in dismutation of O_2^- radicals), and catalase (decomposition of H_2O_2 in water). Biochemical analysis showed that scopolamine group has significantly elevated the levels of MDA (Fig. 6B, $^{***}p < 0.001$), while the

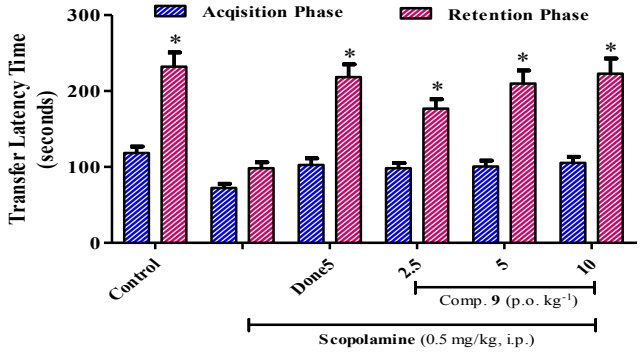

Fig. 5. The effect of compound **9** on scopolamine-induced passive avoidance task in mice. All the results are represented as mean ± SD (n = 6). $^{*}p < 0.05$ compared to respective acquisition test.

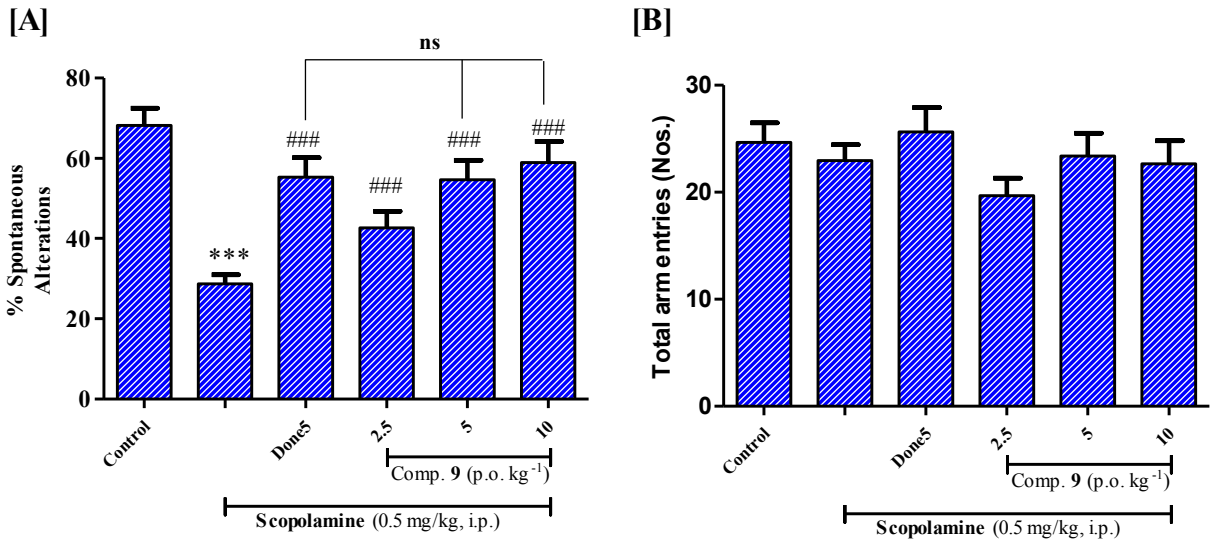

Fig. 4. The effect of compound **9** at the dose of 2.5, 5, and 10 mg/kg, p.o. and donepezil (5 mg/kg, p.o.) by Y-maze test on [A] Spontaneous alteration score (% spontaneous alterations); [B] Total arm entries. All values are represented as mean ± SD (n = 6). $^{***}p < 0.001$ compared to control; $^{\#\#\#}p < 0.001$ compared to scopolamine; ns = non-significant; Done5 = donepezil.

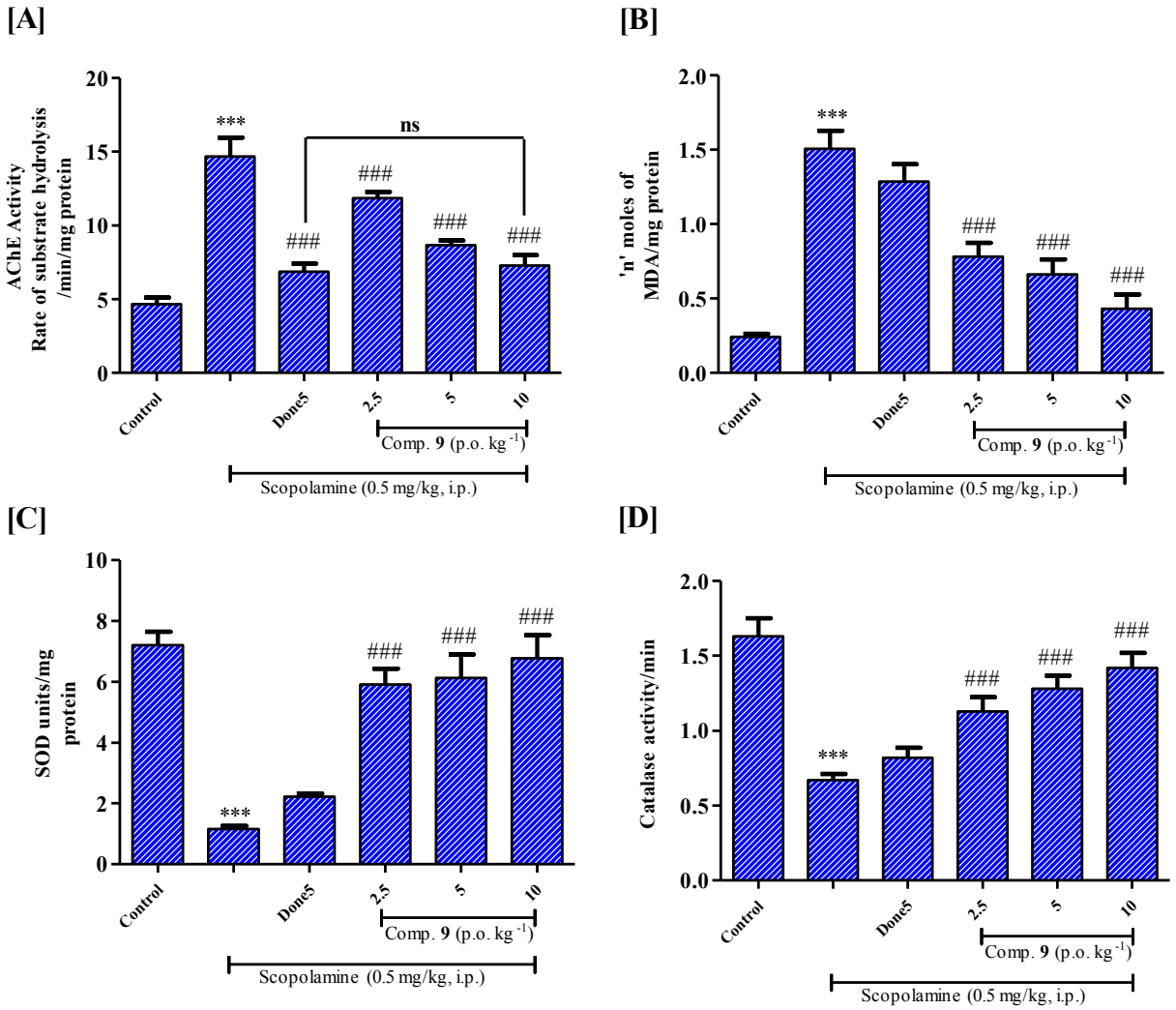

Fig. 6. Effect of compound **9** on the *ex vivo* AChE estimation and biochemical analysis of oxidative stress biomarkers. (A) Ex vivo AChE assay; (B) Lipid peroxidation assay; [C] SOD assay; [D] Catalase assay. All values are expressed as mean ± SD (n = 6). $^{***}p < 0.001$ compared to control, $^{###}p < 0.001$ compared to scopolamine; ns = non-significant; Done5 = donepezil.

levels of SOD (Fig. 6C, $^{***}p < 0.001$) and catalase (Fig. 6D, $^{***}p < 0.001$) were considerably reduced compared to control group. However, the treatment of compound **9** attenuated the levels of MDA (Fig. 6B, $^{###}p < 0.001$), while significantly increasing levels of SOD (Fig. 6C, $^{###}p < 0.001$), and catalase (Fig. 6D, $^{###}p < 0.001$) compared to scopolamine group. Also, the results suggested that donepezil has non-significant antioxidant potential. Overall, the results of *ex vivo* and biochemical analysis suggested compound **9** to possess significant brain AChE inhibitory potential along with antioxidant property.

2.3. Computational analysis

2.3.1. In silico docking studies on AChE

To understand the binding pattern and binding ability of potential compound **9**, docking studies were performed on AChE co-crystallized with donepezil (PDB Code: 1EVE) [49] using Glide module of Schrödinger Maestro 2018-1. The results of binding affinity and interaction pattern were compared with co-crystallized ligand donepezil. The superposition of docked pose of compound **9** and donepezil showed similar binding site interaction and occupancy at the same site of AChE. The most active compound **9** with glide score of −10.6 kcal/mol exhibited several active site interactions (Fig. 7A and B). At the catalytic site, the compound **9** interacted with Ser200 and His440 residues through polar interactions. At anionic subsite, Glu199 residue which is very near to catalytic lining formed H-bonding interaction with the −NH pyridine. The amino acids Trp84 and Phe330 were observed to be involved in π-π stacking with the oxadiazole nucleus. Apart from these interactions, Trp84 also interacted with pyridine ring and −NH pyridine through π-π stacking and π-π cation interactions, respectively. At acyl binding pocket, compound **9** was involved in hydrophobic interactions with the aromatic amino acid residues Phe288, Phe290, and Phe331. At oxyanion hole, Gly117 and Gly118 interacted through glycine interaction. At the peripheral anionic site, compound **9** interacted effectively with the Tyr334, Tyr121 and Asp72 amino acid residues through π-π stacking, hydrophobic and charged interaction, respectively. The detailed interacting residues are also enlisted and given in Table 3.

2.3.2. Molecular dynamics (MD) simulations

The dynamics simulation analysis was carried out with a docked complex of compound **9** and AChE to find out the stability of binding pose in a flexible protein environment having the presence of virtual water molecules. The results of RMSD (root mean square deviation) values for protein and ligand indicated that the system is equilibrated

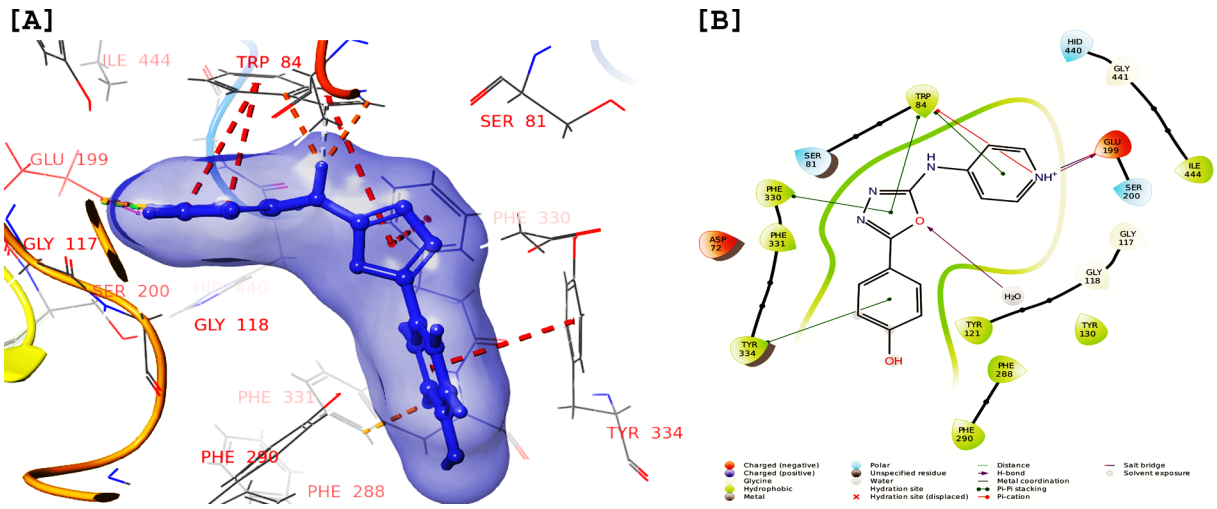

Fig. 7. Docking of compound 9 on AChE. (A) 3D interaction image showing compound **9** in its ligand binding surface interacting with active site residues of AChE represented in ribbon structure; (B) 2D image showing active site interactions.

and fluctuations are within the range of 1–3 Å [42] as compared to reference protein backbone structure. Further, protein and ligand RMSF (root mean square fluctuations) also indicated stable trajectories of ligand and protein residues for the complete simulation run.

The interaction analysis of protein-ligand complex was performed using stacked bar chart and graphical representation. Stacked bar chart analysis showed the interaction fractions for four types: H-bonds, hydrophobic, ionic and water bridge interactions. The interaction of Trp84 showed interaction fraction of more than 1.2 that suggested 120% interaction was maintained for the total simulation run. It also showed that more than 100% interaction was due to multiple contacts of the respective residues (Fig. 8). The graphical representation showed interactions occurred for more than 30% simulation time. The results indicated that H-bonding interactions were maintained with Glu199 and Gly119 for 35% and 38% simulation time, respectively. The interaction with Trp84 through π-π stacking was maintained for 59% simulation time with oxadiazole ring. Also, Tyr334 and Phe331 formed hydrophobic interactions with the respective ligand sites (Fig. 9).

3. Conclusion

The available FDA approved AChEIs could only provide the symptomatic relief to the patient of the AD. The search to find a novel lead for the curative treatment of AD has been failed for a long time and is still the top most priority of medicinal chemists. In our quest to search for a novel lead, a new set of compounds bearing 4-AP nucleus with 1,3,4-oxadiazole ring were designed, synthesized, and characterized by spectroscopic techniques (FT-IR, ^{1}H NMR, and ^{13}C NMR) and elemental analyses. All the results were in agreement with the structures of the synthesized compounds. The results showed non-competitive type of AChE inhibition by compound **9** (IC_{50} = 1.098 μM; Ki = 0.960 μM). The brain permeability and penetration through BBB is the most challenging barrier for the compounds to be effective in the AD. Most of our synthesized analogs except compound **11** showed significant brain permeability through *in vitro* PAMPA-BBB assay. Compound **9** also exhibited excellent inhibitory potential of AChE-induced Aβ aggregation as evaluated by thioflavin T assay at three different ratios of Aβ: inhibitor. Further, *in vivo* behavioral studies were observed for the most potent compound **9** at three doses through Y-maze and passive avoidance tests in mice. The results showed improvement in learning and memory with compound **9** in a dose dependant manner with the maximum effect was observed at the dose of 10 mg/kg, p.o. Moreover, *ex vivo* studies and biochemical analysis were performed, which showed effective AChE inhibition and antioxidant property of compound **9**, respectively. *In silico* molecular docking and dynamics studies displayed consensual binding interactions of compound **9** with catalytic and peripheral anionic site residues of AChE. All these results highlighted the potential of compound **9** to be developed as the significant lead in the development of orally active therapeutics in the treatment of AD.

Table 3
Detailed active site residue interaction analysis of compound 9 and donepezil on AChE.

Comp.	Interacting residues[#]					
	Catalytic site	Peripheral anionic site	Anionic subsite	Acyl binding pocket	Oxyanion hole	Other interacting residues
9	Ser200[a], His440[a]	Tyr334[b], Tyr121[c], Asp72[d]	Glu199[e], Trp84[b,f], Phe330[c]	Phe288[c], Phe290[c], Phe331[c]	Gly117[g], Gly118[g]	Ser81[a], Tyr130[c], Gly441[g], Ile444[c]
Don[*]	Ser200[a], His440[a]	Tyr334[c], Tyr121[c], Asp72[d], Tyr70[c], Trp279[c]	Glu199[d], Trp84[b,f], Phe330[f]	Phe288[c], Phe290[c], Phe331[c]	Gly117[g], Gly118[g]	Tyr130[c], Gly441[g], Ile444[c], Phe331[c], Arg289[d], Ile287[c], Ser286[a], Leu282[c]

[#] All the interacting residues are within the 4 Å distance with the ligand.
[*] Don – Donepezil.
[a] Polar interaction.
[b] π-π stacking interaction.
[c] Hydrophobic interaction.
[d] Charged interaction.
[e] H-bonding interaction.
[f] π-π cation interaction.
[g] Glycine interaction.

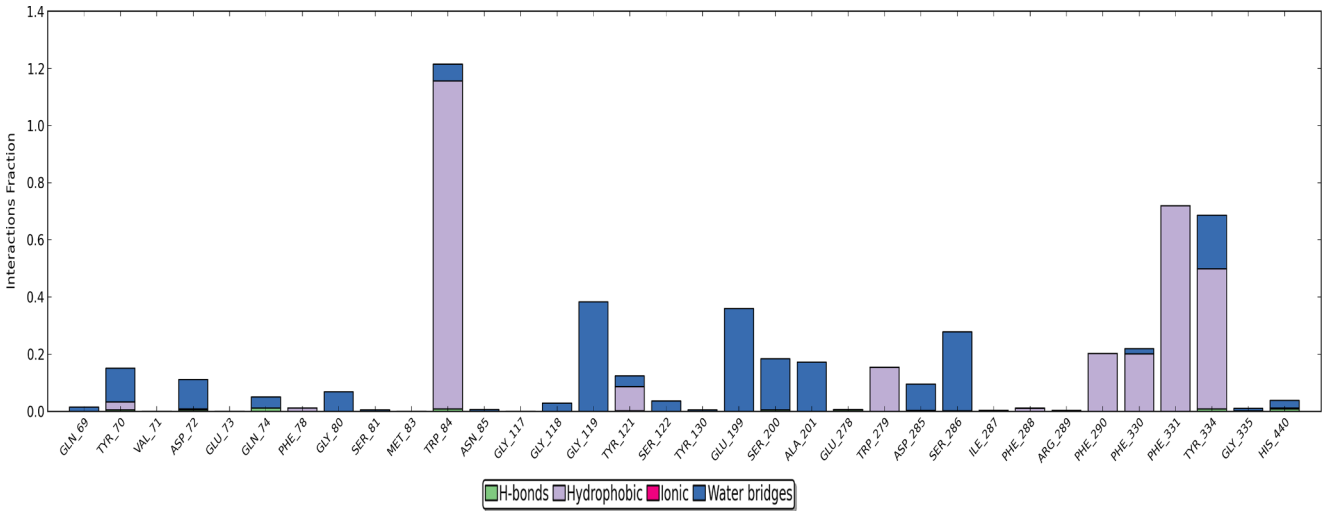

Fig. 8. The detailed interaction fraction analysis of compound **9** and AChE complex.

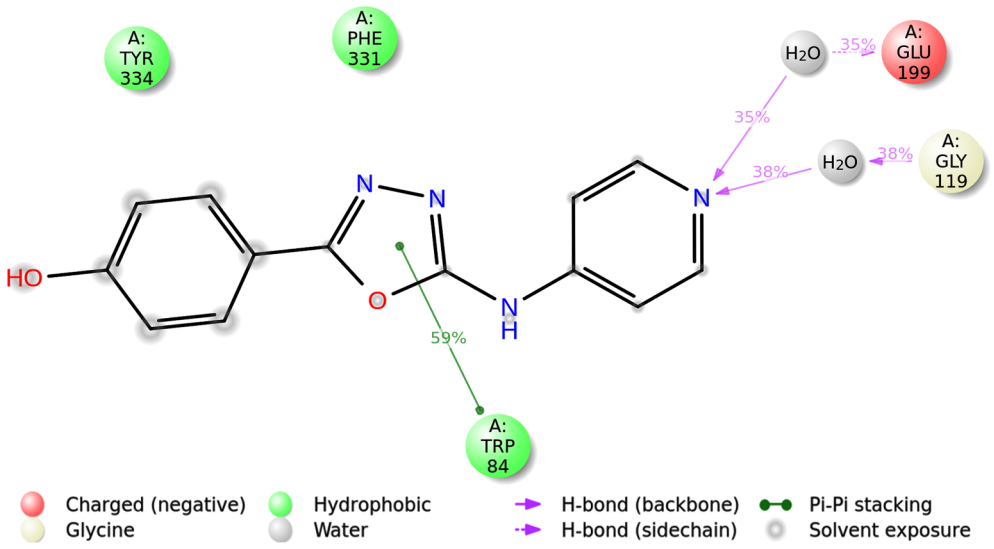

Fig. 9. Graphical representation of compound **9** showing interacting residues with the interaction of more than 30% of total simulation of 30 nsec.

4. Experimental

4.1. Chemicals and instrumentation

All the reagents were commercially available and purchased from Sigma Aldrich. The reaction progresses were monitored, and Rf values were determined using thin layer chromatography (TLC) with pre-coated silica gel plates 60-F254 (Merck, Germany). Open capillary tubes with sealed one end were used to determine the melting points on a Perfit (India) melting point apparatus and were reported as uncorrected. FT-IR spectra were recorded on Bruker ECO-ATR (Alpha) and reported as wavenumber *vs.* % Transmittance. ^{1}H NMR (500 MHz) and ^{13}C NMR (125 MHz) was recorded on a Bruker Avance FT-NMR spectrophotometer at room temperature using TMS as an internal standard. CHN analysis was recorded using EXETER CE-440 elemental analyzer.

4.2. Chemistry

4.2.1. General procedure for the synthesis of (3)

The 4-AP (10 mmol) was dissolved in dichloromethane with pyridine (15 mmol), followed by addition of phenyl chloroformate (11 mmol) at 10 °C and stirred for 24 h at room temperature. The reaction mixture was washed with water (3 × 100 ml), brine, and dried over sodium sulfate. The filtrate was evaporated to get the solid compound (**3**).

Yield: 1.858 g, 87%. FT-IR (ν, cm^{-1}): 3198 (−NH stretching), 1732 (C=O stretching). ^{1}H NMR (DMSO-d_6, ppm): δ 8.55 (d, J = 7.2 Hz, 2H, aromatic CH), 7.64 (d, J = 7.0 Hz, 2H, aromatic CH), 7.28 (t, J = 6.8 Hz, 2H, aromatic CH), 7.18–7.06 (m, 3H, aromatic CH), 5.98 (s, 1H, −NH). ^{13}C NMR (DMSO-d_6, ppm): 156.6, 152.8, 152.7, 151.7, 151.6, 149.2, 130.1, 130.0, 126.2, 123.4, 123.2, 113.3, 113.2. Anal. calc. (%) for $C_{13}H_{10}N_4O$; C, 65.28; H, 4.71; N, 13.08. Found (%): C, 65.68; H, 4.68; N, 13.16.

4.2.2. General procedure for the synthesis of (4) [13].

The compound (**3**, 4.6 mmol) was dissolved in absolute ethanol and hydrazine hydrate (13.8 mmol) were refluxed for 2 h. The reaction mixture was then allowed to cool and solvent was evaporated and crude residue was crystallized with absolute ethanol to afford the pure compound (**4**).

Yield: 0.548 g, 78%. FT-IR (ν, cm^{-1}): 3236, 3234 (−NH_2 stretching), 3198 (−NH stretching). ^{1}H NMR (DMSO-d_6, ppm): δ 8.48 (d, J = 7.4 Hz, 2H, aromatic CH), 7.56 (d, J = 6.8 Hz, 2H, aromatic CH), 6.42 (s, 1H, −NH), 6.22 (s, 1H, −NH), 4.46 (s, 2H, −NH_2). ^{13}C NMR (DMSO-d_6, ppm): 162.3, 153.2, 153.1, 152.7, 114.6, 114.5. Anal. calc. (%) for $C_6H_8N_4O$; C, 47.36; H, 5.30; N, 36.82. Found (%): C, 47.42; H, 5.28; N, 36.78.

*4.2.3. General procedure for the synthesis of (**5–19**).*

Equimolar quantities of various aldehydes and the crystallized product (**4**) were mixed and refluxed for 3–5 h to get semicarbazones. Then, chloramine-T (2.3 equivalents) was added, and stirred for 2–3 h. The reaction solution was cooled and obtained solid was filtered, washed and recrystallized with ethanol to afford the pure 1,3,4-oxadiazole derivatives (**5–19**).

*4.2.3.1. 5-Phenyl-N-(pyridin-4-yl)-1,3,4-oxadiazol-2-amine (**5**).* Yield: 0.188 g, 60.0%. FT-IR (ν, cm^{-1}): 3191 (−NH stretching). ^1H NMR (DMSO-d_6, ppm): δ 9.22 (s, 1H, −NH), 8.39–8.24 (m, 2H, aromatic CH), 7.62–7.50 (m, 4H, aromatic CH), 7.10–6.82 (m, 3H, aromatic CH). ^{13}C NMR (DMSO-d_6, ppm): 162.3, 160.1, 154.2, 151.2, 129.1, 128.3, 126.9, 126.4, 110.2. Anal. calc. (%) for $C_{13}H_{10}N_4O$; C, 65.54; H, 4.23; N, 23.52. Found (%): C, 65.58; H, 4.21; N, 23.49.

*4.2.3.2. 5-(3-Bromophenyl)-N-(pyridin-4-yl)-1,3,4-oxadiazol-2-amine (**6**).* Yield: 0.261 g, 62.8%. FT-IR (ν, cm^{-1}): 3494 (−NH stretching). ^1H NMR (DMSO-d_6, ppm): δ 9.26 (brs, 1H, −NH), 8.32–8.23 (m, 2H, aromatic CH), 7.80–7.41 (m, 3H, aromatic CH), 7.62 (s, 1H, aromatic CH), 7.10–7.02 (m, 2H, aromatic CH). ^{13}C NMR (DMSO-d_6, ppm): 162.2, 160.3, 154.2, 151.2, 133.2, 130.2, 128.4, 126.4, 122.6, 110.5. Anal. calc. (%) for $C_{13}H_9BrN_4O$; C, 49.23; H, 2.86; N, 17.67. Found (%): C, 49.29; H, 2.91; N, 17.71.

*4.2.3.3. 5-(4-Bromophenyl)-N-(pyridin-4-yl)-1,3,4-oxadiazol-2-amine (**7**).* Yield: 0.256 g, 61.7%. FT-IR (ν, cm^{-1}): 3495 (−NH stretching). ^1H NMR (DMSO-d_6, ppm): δ 9.23 (brs, 1H, −NH), 8.33–8.24 (m, 2H, aromatic CH), 7.71–7.62 (m, 4H, aromatic CH), 7.12–7.00 (m, 2H, aromatic CH). ^{13}C NMR (DMSO-d_6, ppm): 162.4, 160.1, 154.3, 151.4, 132.7, 128.8, 125.4, 110.5. Anal. calc. (%) for $C_{13}H_9BrN_4O$; C, 49.23; H, 2.86; N, 17.67. Found (%): C, 49.33; H, 2.88; N, 17.64.

*4.2.3.4. 2-(5-(Pyridin-4-ylamino)-1,3,4-oxadiazol-2-yl)phenol (**8**).* Yield: 0.228 g, 68.3%. FT-IR (ν, cm^{-1}): 3460 (−OH stretching), 3191 (−NH stretching). ^1H NMR (DMSO-d_6, ppm): δ 10.5 (brs, 1H, −OH), 9.21 (s, 1H, −NH); 8.67–8.28 (m, 2H, aromatic CH), 7.65–7.39 (m, 2H, aromatic CH), 7.14–6.89 (m, 4H, aromatic CH). ^{13}C NMR (DMSO-d_6, ppm): δ 161.9, 160.4, 158.1, 154.4, 150.9, 129.7, 126.3, 120.9, 116.5, 109.2, 111.2. Anal. calc. (%) for $C_{13}H_{10}N_4O_2$: C, 61.41; H, 3.96; N, 22.04. Found (%): C, 60.43; H, 3.99; N, 22.01.

*4.2.3.5. 4-(5-(Pyridin-4-ylamino)-1,3,4-oxadiazol-2-yl)phenol (**9**).* Yield: 0.220 g, 65.9%. FT-IR (ν, cm^{-1}): 3358 (−OH stretching), 3261 (−NH stretching). ^1H NMR (DMSO-d_6, ppm): δ 12.98 (brs, 1H, −OH), 9.08 (s, 1H, −NH), 7.95 (d, J = 8.3 Hz, 3H, aromatic CH), 7.62 (t, J = 7.4 Hz, 2H, aromatic CH), 7.51 (d, J = 7.8 Hz, 3H, aromatic CH). ^{13}C NMR (DMSO-d_6, ppm): δ 167.7, 162.3, 159.8, 154.4, 150.9, 117.3, 116.9, 118.4, 109.2; Anal. calc. (%) for $C_{13}H_{10}N_4O_2$: C, 61.41; H, 3.96; N, 22.04. Found (%): C, 60.49; H, 3.92; N, 21.99.

*4.2.3.6. 5-(2-Nitrophenyl)-N-(pyridin-4-yl)-1,3,4-oxadiazol-2-amine (**10**).* Yield: 0.211 g, 56.7%. FT-IR (ν, cm^{-1}): 3194 (−NH stretching). ^1H NMR (DMSO-d_6, ppm): δ 9.23 (s, 1H, −NH), 8.42–8.22 (m, 2H, aromatic CH), 7.79–7.63 (m, 4H, aromatic CH), 7.12–7.09 (m, 2H, aromatic CH). ^{13}C NMR (DMSO-d_6, ppm): δ 162.1, 159.9, 154.2, 150.4, 148.2, 134.8, 131.2, 129.1, 128.2, 123.9, 109.9; Anal. calc. (%) for $C_{13}H_9N_5O_3$: C, 55.13; H, 3.20; N, 24.73. Found (%): C, 55.19; H, 3.17; N, 24.71.

*4.2.3.7. 5-(3-Nitrophenyl)-N-(pyridin-4-yl)-1,3,4-oxadiazol-2-amine (**11**).* Yield: 0.260 g, 69.8%. FT-IR (ν, cm^{-1}): 3196 (−NH stretching). ^1H NMR (DMSO-d_6, ppm): δ 9.27 (s, 1H, −NH), 8.64–8.43 (m, 2H, aromatic CH), 8.16–7.99 (m, 2H, aromatic CH), 7.67–7.58 (m, 4H, aromatic CH). ^{13}C NMR (DMSO-d_6, ppm): δ 162.1, 160, 154.1, 150.1, 148.7, 133.4, 131.9, 129.7, 127.8, 126.0, 111.0. Anal. calc. (%) for $C_{13}H_9N_5O_3$: C, 55.13; H, 3.20; N, 24.73. Found (%): C, 55.16; H, 3.23; N, 24.74.

*4.2.3.8. 5-(4-Nitrophenyl)-N-(pyridin-4-yl)-1,3,4-oxadiazol-2-amine (**12**).* Yield: 0.270 g, 72.4%. FT-IR (ν, cm^{-1}): 3197 (−NH stretching). ^1H NMR (DMSO-d_6, ppm): δ 9.21 (s, 1H, −NH), 8.68–8.27 (m, 4H, aromatic CH), 7.67–7.58 (m, 4H, aromatic CH). ^{13}C NMR (DMSO-d_6, ppm): δ 161.9, 160.2, 154.5, 150.4, 148.2, 132.1, 130.2, 127.9, 111.0. Anal. calc. (%) for $C_{13}H_9N_5O_3$: C, 55.13; H, 3.20; N, 24.73. Found (%): C, 55.11; H, 3.19; N, 24.72.

*4.2.3.9. 5-(3-Chlorophenyl)-N-(pyridin-4-yl)-1,3,4-oxadiazol-2-amine (**13**).* Yield: 0.257 g, 71.8%. FT-IR (ν, cm^{-1}): 3195 (−NH stretching); ^1H NMR (DMSO-d_6, ppm): δ 9.25 (s, 1H, −NH), 8.42–8.31 (m, 2H, aromatic CH), 7.87–7.56 (m, 4H, aromatic CH), 7.04–6.98 (m, 2H, aromatic CH); ^{13}C NMR (DMSO-d_6, ppm): δ 161.2, 160.1, 154.9, 150.1, 135.1, 129.9, 128.8, 127.8, 127.1, 126.1, 111.0; Anal. calc. (%) for $C_{13}H_9ClN_4O$: C, 57.26; H, 3.33; N, 20.55; Found (%): C, 57.27; H, 3.31; N, 20.53.

*4.2.3.10. 5-(4-Chlorophenyl)-N-(pyridin-4-yl)-1,3,4-oxadiazol-2-amine (**14**).* Yield: 0.260 g, 72.6%. FT-IR (ν, cm^{-1}): 3196 (−NH stretching). ^1H NMR (DMSO-d_6, ppm): δ 9.21 (s, 1H, −NH), 8.40–8.35 (m, 2H, aromatic CH), 7.71–7.53 (m, 4H, aromatic CH), 7.01–6.99 (m, 2H, aromatic CH). ^{13}C NMR (DMSO-d_6, ppm): δ 161.4, 160.0, 154.2, 150.4, 134.9, 129.1, 128.4, 124.4, 110.9. Anal. calc. (%) for $C_{13}H_9ClN_4O$: C, 57.26; H, 3.33; N, 20.55. Found (%): C, 57.24; H, 3.29; N, 20.58.

*4.2.3.11. 5-(2,3-Dichlorophenyl)-N-(pyridin-4-yl)-1,3,4-oxadiazol-2-amine (**15**).* Yield: 0.235 g, 58.4%. FT-IR (ν, cm^{-1}): 3193 (−NH stretching). ^1H NMR (DMSO-d_6, ppm): δ 9.12 (s, 1H, −NH), 8.50–8.43 (m, 1H, aromatic CH), 7.88–7.43 (m, 5H, aromatic CH), 7.16–6.94 (m, 1H, aromatic CH). ^{13}C NMR (DMSO-d_6, ppm): δ 158.6, 157.9, 154.2, 152.4, 141.8, 134.2, 133.8, 130.2, 129.8, 129.1, 124.0, 113.32. Anal. calc. (%) for $C_{13}H_8Cl_2N_4O$: C, 50.84; H, 2.63; N, 18.24. Found (%): C, 50.79; H, 2.59; N, 18.21.

*4.2.3.12. N-(pyridin-4-yl)-5-(m-tolyl)-1,3,4-oxadiazol-2-amine (**16**).* Yield: 0.231 g, 69.6%. FT-IR (ν, cm^{-1}): 3191 (−NH stretching). ^1H NMR (DMSO-d_6, ppm): δ 9.15 (s, 1H, −NH), 8.46–8.37 (m, 3H, aromatic CH), 7.98–7.49 (m, 3H, aromatic CH), 7.17–6.99 (m, 2H, aromatic CH), 2.37 (s, 3H, CH_3). ^{13}C NMR (DMSO-d_6, ppm): δ 159.1, 157.9, 154.1, 151.2, 138.9, 130.1, 129.2, 128.9, 126.2, 124.0, 113.2, 23.1. Anal. calc. (%) for $C_{14}H_{12}N_4O$: C, 66.65; H, 4.79; N, 22.21. Found (%): C, 66.67; H, 4.81; N, 22.19.

*4.2.3.13. N-(pyridin-4-yl)-5-(p-tolyl)-1,3,4-oxadiazol-2-amine (**17**).* Yield: 0.223 g, 67.2%. FT-IR (ν, cm^{-1}): 3194 (−NH stretching). ^1H NMR (DMSO-d_6, ppm): δ 9.06 (s, 1H, −NH), 8.44–8.31 (m, 2H, aromatic CH), 7.91–7.31 (m, 4H, aromatic CH), 7.21–7.11 (m, 2H, aromatic CH), 2.34 (s, 3H, CH_3). ^{13}C NMR (DMSO-d_6, ppm): δ 159.0, 157.3, 154.7, 151.0, 130.6, 129.2, 127.1, 126.8, 123.7, 111.9, 23.4. Anal. calc. (%) for $C_{14}H_{12}N_4O$: C, 66.65; H, 4.79; N, 22.21. Found (%): C, 66.61; H, 4.83; N, 22.24.

*4.2.3.14. 5-(4-Methoxyphenyl)-N-(pyridin-4-yl)-1,3,4-oxadiazol-2-amine (**18**).* Yield: 0.228 g, 64.6%. FT-IR (ν, cm^{-1}): 3491 (−NH stretching). ^1H NMR (DMSO-d_6, ppm): δ 9.08 (s, 1H, −NH), 8.45–8.37 (m, 2H, aromatic CH), 7.72–7.70 (m, 2H, aromatic CH), 7.19–7.03 (m, 4H, aromatic CH), 3.73 (s, 3H, OCH_3). ^{13}C NMR (DMSO-d_6, ppm): δ 163.1, 159.7, 157.2, 154.2, 151.5, 132.2, 130.5, 129.7, 126.1, 114.2, 111.0, 55.9. Anal. calc. (%) for $C_{14}H_{12}N_4O_2$: C, 62.68; H, 4.51; N, 20.88. Found (%): C, 62.59, H 4.53, N, 20.92.

*4.2.3.15. N-(pyridin-4-yl)-5-(3,4,5-trimethoxyphenyl)-1,3,4-oxadiazol-2-amine (**19**).* Yield: 0.288 g, 66.7%. FT-IR (ν, cm^{-1}): 3494 (−NH

stretching). ^{1}H NMR (DMSO-d_6, ppm): δ 9.08 (s, 1H, −NH), 8.41–8.36 (m, 2H, aromatic CH), 7.30 (s, 2H, aromatic CH), 7.11–7.01 (m, 2H, aromatic CH), 3.75 (s, 3H, OCH_3), 3.65 (s, 6H, $OCH_3 \times 2$). ^{13}C NMR (DMSO-d_6, ppm): δ 159.2, 157.1, 154.0, 153.4, 151.2, 138.1, 120.1, 111.5, 104.5, 58.4, 55.2. Anal. calc. (%) for $C_{16}H_{16}N_4O_4$: C, 58.53; H, 4.91; N, 17.06. Found (%): C, 58.48; H, 4.94; N, 17.03.

4.3. Determination of LogP values: Shake flask method

The lipophilic constant of all the synthesized compounds (**5–19**) was determined in *n*-octanol and buffer (pH 7.4) by the shake flask method. The log P was calculated by correlating the absorbance with the concentration using a standard plot [28].

4.4. Pharmacology

4.4.1. Cholinesterase inhibition assay [40,50]

The *in vitro* cholinesterase inhibitory potency against AChE and BChE was determined for all the synthesized compounds using Ellman colorimetric assay. All the assay solutions were prepared in 0.1 M phosphate buffer solution at pH 7.4 except the test compounds, which were prepared in biological grade DMSO (final concentration < 1% v/v). The final assay solutions consisted of 340 μM 5,5′-dithiobis(2-nitrobenzoic acid) (DTNB), 2.5 units/ml of hAChE (AChE from human erythrocytes, Sigma EC No. 3.1.1.7) or hBChE (BChE from human serum, Sigma EC No. 3.1.1.8) at varied concentrations of test compounds (10 nM to 10 μM) in biological grade DMSO, and 550 μM of acetylthiocholine iodide (ATCI) or butyrylthiocholine iodide (BTCI) as substrate for AChE and BChE, respectively. Initially, the test compounds were pre-incubated with enzyme for 10 min at room temperature. After that period, DTNB and substrate were added, and absorbance was measured at 412 nm for 6 min using H1M synergy multimode microplate reader. Donepezil was used as a positive reference standard. The reaction rates were compared, and the percentage inhibition due to the presence of test compounds was calculated with respective IC_{50} values using graph pad prism version 5.01. The IC_{50} values can be designed as the concentration of test inhibitors responsible for 50% inhibition of enzyme action as compared to control (without inhibitors). All results are determined as the mean of three independent measurements.

4.4.2. Enzyme kinetics [51]

The Lineweaver-Burk method was used to determine the mechanism of enzyme inhibition using the different concentrations of substrate and a fixed quantity of hAChE, in the absence or presence of inhibitor. The concentration of inhibitor was selected by its IC_{50} value. Compound **9** was used in three different concentration range (1, 1.5, and 2 μM). Each concentration of inhibitor was evaluated with six different concentrations of ATCI. The values of V_{max} and K_m were calculated using Michaelis-Menten non-linear regression kinetics, and the mechanism of enzyme inhibition was determined by Lineweaver-Burk plots [51] using Graph Pad Prism 5.01. The inhibitory constant Ki value was determined by the Cheng–Prusoff equation [52].

4.4.3. PAMPA-BBB assay [43,48]

The permeability of synthesized compounds across the blood-brain barrier (BBB) was assessed by PAMPA-BBB assay. The protocol of PAMPA-BBB assay involved the coating of acceptor microplate (PTFE, 0.45 μm, Merck Millipore) with 4 μl of 20 mg/ml porcine brain lipid (Avanti polar lipids) in dodecane (Avra synthesis). After coating, 200 μl of pH 7.4 buffer was taken in acceptor microplates. Test compounds were initially dissolved in DMSO and further diluted with pH 7.4 buffer to prepare 25 μg/ml concentration. 200 μl of the test solution was taken in a donor microplate (Merck Millipore). The donor microplate placed carefully like a sandwich over acceptor microplate and 18 h incubation period was initiated. Spectrophotometrically using H1M synergy multimode microplate reader (Biotek, USA) concentration of test compounds were determined in acceptor and donor microplates. The model was validated using standard commercial drug samples.

4.4.4. Amyloid beta aggregation inhibition: Thioflavin T assay

$A\beta_{1\text{-}42}$ (Sigma, India) was dissolved in 1% v/v ammonium hydroxide solution to get the 2000 μM stock solution and stored at −80 °C. The test compound was initially dissolved in DMSO, and final dilutions were made in PBS pH 7.4. Different proportion of $A\beta_{1\text{-}42}$: inhibitor was tested (10:5, 10:10; and 10:20 μM) by thioflavin T assay [48,53,54]. All the experiments were performed in triplicates. The mixture of $A\beta_{1\text{-}42}$ (final concentration 10 μM, 2 μl) and AChE from human erythrocytes (final concentration 230 μM, 16 μl) were incubated with or without tested compound (5 μM, 10 μM, and 20 μM; 2 μl) at 37 °C for 48 h. The fluorescence intensities were measured with the addition of 50 mM glycine-NaOH buffer (pH 8.0) containing 5 μM thioflavin T at the excitation and emission wavelength of λ_{ex} = 450 nm and λ_{em} = 485 nm, respectively. The percentage inhibition was calculated using the following expression: $100–(IF_i/IF_0 \times 100)$, where IF_i and IF_0 are the fluorescence intensities with and without inhibitor, respectively after subtracting the values with the blank. The results were also reported as normalized fluorescence intensity with respect to control.

4.4.5. In vivo studies

4.4.5.1. Animals. The behavioral studies were conducted on male Albino mice (adult male, 25–30 g). These mice were bought from Central Animal Facility, IMS (BHU), Varanasi, India. Mice were kept in six per polyacrylic cage with semi-synthetic balanced diet, water, temperature and relative humidity of the storage room was maintained to 25 ± 2 °C and 55 ± 10%, respectively under 12 h light/dark rotations. Mice were maintained and treated according to CPCSEA guidelines. The study protocols and quantity of mice were duly permitted by the IAEC (Dean/2017/CAEC/88]. Different animals were used for each behavioral investigation.

4.4.5.2. Experimental design. Animals were adapted to the laboratory conditions 7 days before behavioral studies. Scopolamine hydrobromide solution was prepared by dissolving it in distilled water, and amnesia was induced by its intraperitoneal administration of scopolamine (0.5 mg/kg) on the 7th day, 1 h after the administration of treatment. The behavioral studies were performed just after 5 min of scopolamine administration. Donepezil hydrochloride and compound **6g** were suspended in the 0.3% w/v sodium carboxymethyl cellulose (CMC). The animals were divided into six groups for the behavioral experiment. Each group having six mice as following: (i) control, (ii) scopolamine (0.5 mg/kg, i.p.), (iii) donepezil (5 mg/kg, p.o.) as a reference standard, (iv) compound **9** (2.5 mg/kg) (v) compound **9** (5 mg/kg) (vi) compound **9** (10 mg/kg). Donepezil and compound **9** were given orally (*p.o.*) once daily for seven consecutive days to all respective groups except for the control and scopolamine group. Scopolamine group of animals were given vehicle treatment for seven days. The behavioral studies were accomplished by Y-maze and passive avoidance tests.

4.4.5.3. Y-maze test [55]. The immediate working memory of the rodents can be assessed by the Y-maze test. Compound **9** and standard (donepezil) in specifically mentioned doses were administered for seven days. After 5 min of scopolamine injection on the 7th day of the treatment, the main experiment was performed in which each mouse was placed at the center of the three arms for fifteen minutes and observed by the camera for the total number of arms entries. The repeated arm entries indicate the memory dysfunction. The successive choices of each arm (i.e., ABC, BCA, or CAB but not BAB, ABB) and entry through the novel arm could be considered as an improvement in memory dysfunctions. The memory improvement score was calculated using the % spontaneous alterations = (Number of spontaneous alterations/(total arm entries) – 2)) × 100.

4.4.5.4. Passive avoidance test [56]. Passive avoidance test provides a good measure to evaluate the learning and memory in rodents. The instrument was fabricated with two light and dark compartment boxes having dimensions of 12 × 10 × 12 cm. Both the boxes were connected with door and stainless steel electric bar of 2 mm size placed at a distance of 0.5 cm. The current flow and voltage of the system were regulated to 0.05 mA and 20 V, respectively. The main experiment was performed into two phases: the first phase involved the acquisition test, and next phase includes retention test. Both phases should have one day phase interval in between each other. The tests were conducted for the total period of 300 sec. After the once-daily administration of test compounds for the 7 days, the training period was initiated on last day after 5 min of intraperitoneal injection of scopolamine hydrobromide. Acquisition phase involved the exposure of each mouse in the light chamber followed by the opening of dark compartment entry. As soon as mouse entered the dark compartment, the door was closed. Further, the medium intensity foot shock of 0.05 mA was applied for 2 sec through stainless steel electric bar. After one day of the acquisition phase, the mouse was again placed in the light chamber and monitored for entering in the dark chamber within next 300 sec. The period taken by each mouse to enter in the dark chamber was considered as their TL. During retention test, foot shock was not applied to prevent reacquisition.

4.4.6. Dissection and homogenization

After completion of behavioral studies, mice were sacrificed through cervical dislocation after paralyzing them using diethyl ether. The whole brains were immediately isolated and washed with cold saline (0.9% w/v). Each whole brain and 3 ml of 10 mM cold sodium phosphate buffer pH 7.4 were homogenized in the Teflon-glass homogenizer and centrifuged at 2–8 °C for 10 min at 11,000 rpm to get the homogenates. Further, the collected homogenates were used to analyze the various biochemical parameters.

4.4.7. Ex vivo estimation of AChE [40,57]

Ellman method was used to determine the level of a cholinergic biomarker, AChE in the whole brain homogenate. The protocol was based upon the reaction between the hydrolyzed product of ATCI, thiocholine, and DTNB to produce a yellow colored product, which was estimated at 412 nm spectrophotometrically. The assay solution of 25 µl of tissue homogenate, 150 µl of 0.1 M phosphate buffer pH 7.4, and 100 µl of 10 mM DTNB were preincubated for 10 min at room temperature. The reaction was initiated by the addition of 20 µl of 75 mM ATCI and absorbance was measured at 412 nm. The expression of AChE inhibitory potency was reported as hydrolyzed substrate.

4.4.8. Biochemical analysis

4.4.8.1. Lipid peroxidation assay [58,59]. The antioxidant potential was evaluated by TBARS assay, also known as a lipid peroxidation assay. Initially, 0.5 ml of brain homogenate was preincubated in 0.5 ml of Tris HCl pH 8.0 buffer at 37 °C for 2 h followed by addition of 1 ml of 10% v/v ice-cold trichloroacetic acid solution. The reaction mixture was further centrifuged at 1000 rpm for 10 min, and the 1 ml of supernatant was mixed with 1 ml thiobarbituric acid (TBA). The reaction mixture was warmed in a hot water bath for 10 min and cooled. Further, 1 ml of double distilled water was added and the optical density of the solution was measured at 532 nm. The intensity of the pink color of the TBARS is proportional to the level of lipid peroxidation in the homogenate. The results were calculated as a number of moles of MDA/mg protein.

4.4.8.2. SOD assay [60]. The SOD assay was carried out according to the already reported protocol reported by Kono in 1978. The test solution comprised of 0.1 mM ethylenediamine tetraacetic acid, 96 mM nitroblue tetrazolium, and 50 mM sodium carbonate. The above mixture (2 ml), 0.05 ml brain homogenate, and 0.05 ml of hydroxylamine hydrochloride (pH 6.0 maintained using NaOH) were taken in a cuvette, and the change in optical density was measured at 560 nm for 2 min at 30 sec interval.

4.4.8.3. Catalase assay [61]. The catalase activity assay was performed by mixing 1.95 ml of 0.1 M phosphate buffer pH 7.4, 1 ml of 19 mM H_2O_2, and 0.05 ml of brain homogenate to make a final assay volume of 3.0 ml. The absorbance change was measured at 240 nm, and the results were calculated as mM of catalase activity responsible for decomposition of H_2O_2/min/mg protein.

4.5. Computational studies

4.5.1. In silico docking simulations

The *in silico* molecular docking study for compound **9** was performed using Schrödinger Maestro 2018-1 version on HP Kernel Linux workstation and the results of docking studies were compared with standard and co-crystallized ligand donepezil. AChE enzyme structure with co-crystallized ligand donepezil (PDB Code: 1EVE) from the organism *Tetronarce Californica* was used for the docking study [49]. Protein preparation wizard module of Schrödinger Maestro was used to prepare the enzyme structure. Protein structure was downloaded from RCSB data bank and preprocessed firstly to assign bond orders, add hydrogens, and create disulfide bonds. Further using the Prime module, missing side chains and loops were filled. The water molecules beyond the 5 Å distance from ligand were removed. The possible states of preprocessed protein structure were generated at pH 7.0 ± 3.0 and state with lower penalty score was used for further optimizing using PROPKA method at pH 7.0. The protein structure was minimized using force field OPLS_2005 by converging heavy atoms RMSD to 0.3 Å. Using the LigPrep module, all the possible conformers of ligand molecules were generated and minimized using an OPLS_2005 force field. The EPIK method was used to generate possible states of all the conformers at pH 7.0 ± 2.0. Receptor Grid Generation protocol was used to generate the active site grid surrounding the co-crystallized ligand. The 10 Å grid box was generated around the co-crystallized ligand, and all other parameters were kept at default values. Further, to validate the generated grid and docking protocols, co-crystallized ligand donepezil was split from protein structure and re-docked using XP glide module. The re-docked pose of donepezil was compared with co-crystallized pose using the superposition tool, and the RMSD value was calculated, which was found to be within the range of 2 Å. Glide XP module was used to perform the docking, and the results were analyzed using the Glide XP visualizer function.

4.5.2. MD simulations

To affirm the binding stability of docked pose of compound **9**-AChE complex, 30 ns MD simulation run was performed using the Desmond module embedded in Schrödinger Maestro 2015-2 Version. Firstly, the system of the docked complex was built using a system builder tool. Virtual water molecules were added by forming orthorhombic box surrounding the whole protein-ligand complex using the TIP3P model. The total of 15,964 water molecules was added to build the system with total 56,520 atoms. The system was neutralized by addition of 9 Na^+ ions and salt was added at a concentration of 0.15 M. The built system was minimized using 2000 maximum iterations and 1.0 kcal/mol/Å convergence threshold. The dynamics simulation run of 30 ns was performed by keeping the recording interval of 30 ps with a total of 1000 frames. The constant number of atoms (N), pressure (P), and the temperature was maintained (T). The temperature was kept to 300 K and pressure was adjusted to 1.01325 bar.

Declaration of Competing Interest

Authors declare no conflict of interest.

Acknowledgments

The authors are thankful to Department of Health Research (DHR), Ministry of Health and Family Welfare (MHFW), Govt. of India, New Delhi for providing financial assistance through Young Scientist grant in newer areas of Drugs Chemistry (V25011/215-HRD/2016-HR).

References

[1] J. Hugo, M. Ganguli, Dementia and cognitive impairment: epidemiology, diagnosis, and treatment, Clin. Geriatr. Med. 30 (3) (2014) 421–442.
[2] P. Piplani, A. Jain, D. Devi, A. Sharma, P. Silakari, Design, synthesis and pharmacological evaluation of some novel indanone derivatives as acetylcholinesterase inhibitors for the management of cognitive dysfunction, Biorg. Med. Chem. 26 (1) (2018) 215–224.
[3] A.L. Sosa-Ortiz, I. Acosta-Castillo, M.J. Prince, Epidemiology of dementias and Alzheimer's disease, Arch. Med. Res. 43 (8) (2012) 600–608.
[4] C. Patterson, World Alzheimer Report 2018, The state of the art of dementia research, New frontiers, Alzheimer's Disease International, World Alzheimer Report 2018, 2018.
[5] P.N. Tripathi, P. Srivastava, P. Sharma, A. Seth, S.K. Shrivastava, Design and development of novel N-(pyrimidin-2-yl)-1, 3, 4-oxadiazole hybrids to treat cognitive dysfunctions, Biorg. Med. Chem. 27 (7) (2019) 1327–1340.
[6] J. Folch, D. Petrov, M. Ettcheto, S. Abad, E. Sánchez-López, M.L. García, J. Olloquequi, C. Beas-Zarate, C. Auladell, A. Camins, Current research therapeutic strategies for Alzheimer's disease treatment, Neural Plast. 2016 (2016).
[7] J. Godyń, J. Jończyk, D. Panek, B. Malawska, Therapeutic strategies for Alzheimer's disease in clinical trials, Pharmacol. Rep. 68 (1) (2016) 127–138.
[8] P. Munoz-Ruiz, L. Rubio, E. García-Palomero, I. Dorronsoro, M. del Monte-Millán, R. Valenzuela, P. Usán, C. de Austria, M. Bartolini, V. Andrisano, Design, synthesis, and biological evaluation of dual binding site acetylcholinesterase inhibitors: new disease-modifying agents for Alzheimer's disease, J. Med. Chem. 48 (23) (2005) 7223–7233.
[9] A. Kumar, C.M. Nisha, C. Silakari, I. Sharma, K. Anusha, N. Gupta, P. Nair, T. Tripathi, A. Kumar, Current and novel therapeutic molecules and targets in Alzheimer's disease, J. Formosan Med. Assoc. 115 (1) (2016) 3–10.
[10] L.F.N. Lemes, G. de Andrade Ramos, A.S. de Oliveira, F.M.R. da Silva, G. de Castro Couto, M. da Silva Boni, M.J.R. Guimarães, I.N.O. Souza, M. Bartolini, V. Andrisano, Cardanol-derived AChE inhibitors: towards the development of dual binding derivatives for Alzheimer's disease, Eur. J. Med. Chem. 108 (2016) 687–700.
[11] R.-S. Li, X.-B. Wang, X.-J. Hu, L.-Y. Kong, Design, synthesis and evaluation of flavonoid derivatives as potential multifunctional acetylcholinesterase inhibitors against Alzheimer's disease, Bioorg. Med. Chem. Lett. 23 (9) (2013) 2636–2641.
[12] P. Srivastava, P.N. Tripathi, P. Sharma, S.N. Rai, S.P. Singh, R.K. Srivastava, S. Shankar, S.K. Shrivastava, Design and development of some phenyl benzoxazole derivatives as a potent acetylcholinesterase inhibitor with antioxidant property to enhance learning and memory, Eur. J. Med. Chem. 163 (2019) 116–135.
[13] S.K. Sinha, S.K. Shrivastava, Synthesis, evaluation and molecular dynamics study of some new 4-aminopyridine semicarbazones as an antiamnesic and cognition enhancing agents, Biorg. Med. Chem. 21 (17) (2013) 5451–5460.
[14] S.K. Sinha, S.K. Shrivastava, Synthesis and evaluation of some new 4-aminopyridine derivatives as a potent antiamnesic and cognition enhancing drugs, Med. Chem. Res. 21 (12) (2012) 4395–4402.
[15] D.-M. Wang, B. Feng, H. Fu, A.-L. Liu, L. Wang, G.-H. Du, S. Wu, Design, synthesis, and biological evaluation of a new series of biphenyl/bibenzyl derivatives functioning as dual inhibitors of acetylcholinesterase and butyrylcholinesterase, Molecules 22 (1) (2017) 172.
[16] S.K. Shrivastava, S.K. Sinha, P. Srivastava, P.N. Tripathi, P. Sharma, M.K. Tripathi, A. Tripathi, P.K. Choubey, D.K. Waiker, L.M. Aggarwal, M. Dixit, S.C. Kheruka, S. Gambhir, S. Shankar, R.K. Srivastava, Design and development of novel p-aminobenzoic acid derivatives as potential cholinesterase inhibitors for the treatment of alzheimer's disease, Bioorg. Chem. 82 (2018) 211–223.
[17] P. Sharma, P. Srivastava, A. Seth, P.N. Tripathi, A.G. Banerjee, S.K. Shrivastava, Comprehensive review of mechanisms of pathogenesis involved in Alzheimer's disease and potential therapeutic strategies, Prog. Neurobiol. 174 (2018) 53–89.
[18] P.N. Tripathi, P. Srivastava, P. Sharma, M.K. Tripathi, A. Seth, A. Tripathi, S.N. Rai, S.P. Singh, S.K. Shrivastava, Biphenyl-3-oxo-1, 2, 4-triazine linked piperazine derivatives as potential cholinesterase inhibitors with anti-oxidant property to improve the learning and memory, Bioorg. Chem. 85 (2019) 82–96.
[19] M. Bartolini, C. Bertucci, V. Cavrini, V. Andrisano, β-Amyloid aggregation induced by human acetylcholinesterase: inhibition studies, Biochem. Pharmacol. 65 (3) (2003) 407–416.
[20] P. Sharma, A. Tripathi, P.N. Tripathi, S.K. Prajapati, A. Seth, M.K. Tripathi, P. Srivastava, V. Tiwari, S. Krishnamurthy, S.K. Shrivastava, Design and development of multitarget-directed N-Benzylpiperidine analogs as potential candidates for the treatment of Alzheimer's disease, Eur. J. Med. Chem. 167 (2019) 510–524.
[21] P. Mao, P.H. Reddy, Aging and amyloid beta-induced oxidative DNA damage and mitochondrial dysfunction in Alzheimer's disease: implications for early intervention and therapeutics, Biochim. Biophys. Acta Mol. Basis Dis. 1812 (11) (2011) 1359–1370.
[22] A.-U. Rehman, K. Nafeesa, M.A. Abbasi, S.Z. Siddiqui, S. Rasool, S.A.A. Shah, M. Ashraf, Synthesis of new heterocyclic 3-piperidinyl-1, 3, 4-oxadiazole derivatives as potential drug candidate for the treatment of Alzheimer's disease, Cogent Chem. 4 (1) (2018) 1472197.
[23] W.-W. Mei, S.-S. Ji, W. Xiao, X.-D. Wang, C.-S. Jiang, W.-Q. Ma, H.-Y. Zhang, J.-X. Gong, Y.-W. Guo, Synthesis and biological evaluation of benzothiazol-based 1, 3, 4-oxadiazole derivatives as amyloid β-targeted compounds against Alzheimer's disease, Monatshefte für Chemie-Chemical Monthly 148 (10) (2017) 1807–1815.
[24] M. Mohammadi-Khanaposhtani, M. Mahdavi, M. Saeedi, R. Sabourian, M. Safavi, M. Khanavi, A. Foroumadi, A. Shafiee, T. Akbarzadeh, Design, synthesis, biological evaluation, and docking study of acetylcholinesterase inhibitors: new acridone-1, 2, 4-oxadiazole-1, 2, 3-triazole hybrids, Chem. Biol. Drug Des. 86 (6) (2015) 1425–1432.
[25] A. Andreani, A. Leoni, A. Locatelli, R. Morigi, M. Rambaldi, C. Pietra, G. Villetti, 4-Aminopyridine derivatives with antiamnesic activity, Eur. J. Med. Chem. 35 (1) (2000) 77–82.
[26] S.K. Sinha, S.K. Shrivastava, Design, synthesis and evaluation of some new 4-aminopyridine derivatives in learning and memory, Bioorg. Med. Chem. Lett. 23 (10) (2013) 2984–2989.
[27] V.R. Solomon, C. Hu, H. Lee, Hybrid pharmacophore design and synthesis of isatin–benzothiazole analogs for their anti-breast cancer activity, Biorg. Med. Chem. 17 (21) (2009) 7585–7592.
[28] A.G. Banerjee, N. Das, S.A. Shengule, P.A. Sharma, R.S. Srivastava, S.K. Shrivastava, Design, synthesis, evaluation and molecular modelling studies of some novel 5, 6-diphenyl-1, 2, 4-triazin-3 (2H)-ones bearing five-member heterocyclic moieties as potential COX-2 inhibitors: a hybrid pharmacophore approach, Bioorg. Chem. 69 (2016) 102–120.
[29] M. Davidson, Z. Zemishlany, R.C. Mohs, T.B. Horvath, P. Powchik, J.P. Blass, K.L. Davis, 4-Aminopyridine in the treatment of Alzheimer's disease, Biol. Psychiatry 23 (5) (1988) 485–490.
[30] G. Şahin, E. Palaska, M. Ekizoğlu, M. Özalp, Synthesis and antimicrobial activity of some 1, 3, 4-oxadiazole derivatives, Il Farmaco 57 (7) (2002) 539–542.
[31] S.S. Thakkar, P. Thakor, H. Doshi, A. Ray, 1, 2, 4-triazole and 1, 3, 4-oxadiazole analogues: synthesis, MO studies, in silico molecular docking studies, antimalarial as DHFR inhibitor and antimicrobial activities, Biorg. Med. Chem. 25 (15) (2017) 4064–4075.
[32] B. Yadagiri, S. Gurrala, R. Bantu, L. Nagarapu, S. Polepalli, G. Srujana, N. Jain, Synthesis and evaluation of benzosuberone embedded with 1,3,4-oxadiazole, 1,3,4-thiadiazole and 1,2,4-triazole moieties as new potential anti proliferative agents, Bioorg. Med. Chem. Lett. 25 (10) (2015) 2220–2224.
[33] M.A. Tantray, I. Khan, H. Hamid, M.S. Alam, A. Dhulap, A. Kalam, Synthesis of benzimidazole-linked-1,3,4-oxadiazole carboxamides as GSK-3β inhibitors with in vivo antidepressant activity, Bioorg. Chem. 77 (2018) 393–401.
[34] M.Y. Wani, A. Ahmad, R.A. Shiekh, K.J. Al-Ghamdi, A.J. Sobral, Imidazole clubbed 1,3,4-oxadiazole derivatives as potential antifungal agents, Biorg. Med. Chem. 23 (15) (2015) 4172–4180.
[35] W. Wu, Q. Chen, A. Tai, G. Jiang, G. Ouyang, Synthesis and antiviral activity of 2-substituted methylthio-5-(4-amino-2-methylpyrimidin-5-yl)-1,3,4-oxadiazole derivatives, Bioorg. Med. Chem. Lett. 25 (10) (2015) 2243–2246.
[36] A.G. Banerjee, N. Das, S.A. Shengule, R.S. Srivastava, S.K. Shrivastava, Synthesis, characterization, evaluation and molecular dynamics studies of 5, 6–diphenyl–1, 2, 4–triazin–3 (2H)–one derivatives bearing 5–substituted 1, 3, 4–oxadiazole as potential anti–inflammatory and analgesic agents, Eur. J. Med. Chem. 101 (2015) 81–95.
[37] H.L. Yale, K. Losee, 2-Amino-5-substituted 1, 3, 4-oxadiazoles and 5-imino-2-substituted Δ2-1, 3, 4-oxadiazolines. A group of novel muscle relaxants, J. Med. Chem. 9(4) (1966) 478–483.
[38] K.M. Khan, M. Ashraf, I. Ahmad, S.A. Ejaz, Synthesis, characterization and biological screening of 5-substituted-1, 3, 4-oxadiazole-2yl-N-(2-methoxy-5-chlorophenyl)-2-sulfanyl acetamide, Pak. J. Pharm. Sci. 26 (2) (2013) 345–352.
[39] A. Kamal, A.B. Shaik, G.N. Reddy, C.G. Kumar, J. Joseph, G.B. Kumar, U. Purushotham, G.N. Sastry, Synthesis, biological evaluation, and molecular modeling of (E)-2-aryl-5-styryl-1, 3, 4-oxadiazole derivatives as acetylcholine esterase inhibitors, Med. Chem. Res. 23 (4) (2014) 2080–2092.
[40] G.L. Ellman, K.D. Courtney, V. Andres Jr, R.M. Featherstone, A new and rapid colorimetric determination of acetylcholinesterase activity, Biochem. Pharmacol. 7 (2) (1961) 88–95.
[41] M. Kumar, P. Sharma, R. Maheshwari, M. Tekade, S.K. Shrivastava, R.K. Tekade, Beyond the Blood–Brain Barrier: Facing New Challenges and Prospects of Nanotechnology-Mediated Targeted Delivery to the Brain, Nanotechnology-Based Targeted Drug Delivery Systems for Brain Tumors, Elsevier, 2018, pp. 397–437.
[42] A. Seth, P.A. Sharma, A. Tripathi, P.K. Choubey, P. Srivastava, P.N. Tripathi, S.K. Shrivastava, Design, synthesis, evaluation and molecular modeling studies of some novel N-substituted piperidine-3-carboxylic acid derivatives as potential anticonvulsants, Med. Chem. Res. 27 (4) (2018) 1206–1225.
[43] L. Di, E.H. Kerns, K. Fan, O.J. McConnell, G.T. Carter, High throughput artificial membrane permeability assay for blood–brain barrier, Eur. J. Med. Chem. 38 (3) (2003) 223–232.
[44] N.C. Inestrosa, A. Alvarez, C.A. Perez, R.D. Moreno, M. Vicente, C. Linker, O.I. Casanueva, C. Soto, J. Garrido, Acetylcholinesterase accelerates assembly of amyloid-β-peptides into Alzheimer's fibrils: possible role of the peripheral site of the enzyme, Neuron 16 (4) (1996) 881–891.
[45] E. Nepovimova, E. Uliassi, J. Korabecny, L.E. Pena-Altamira, S. Samez, A. Pesaresi, G.E. Garcia, M. Bartolini, V. Andrisano, C. Bergamini, Multitarget drug design strategy: quinone–tacrine hybrids designed to block amyloid-β aggregation and to exert anticholinesterase and antioxidant effects, J. Med. Chem. 57 (20) (2014) 8576–8589.
[46] I. Klinkenberg, A. Blokland, The validity of scopolamine as a pharmacological model for cognitive impairment: a review of animal behavioral studies, Neurosci.

Biobehav. Rev. 34 (8) (2010) 1307–1350.
[47] A. Wolf, B. Bauer, E.L. Abner, T. Ashkenazy-Frolinger, A.M. Hartz, A comprehensive behavioral test battery to assess learning and memory in 129S6/Tg2576 mice, PLoS ONE 11 (1) (2016) e0147733.
[48] D. Kumar, S.K. Gupta, A. Ganeshpurkar, G. Gutti, S. Krishnamurthy, G. Modi, S.K. Singh, Development of Piperazinediones as dual inhibitor for treatment of Alzheimer's disease, Eur. J. Med. Chem. 150 (2018) 87–101.
[49] G. Kryger, I. Silman, J.L. Sussman, Structure of acetylcholinesterase complexed with E2020 (Aricept®): implications for the design of new anti-Alzheimer drugs, Structure 7 (3) (1999) 297–307.
[50] S.K. Shrivastava, P. Srivastava, T. Upendra, P.N. Tripathi, S.K. Sinha, Design, synthesis and evaluation of some N-methylenebenzenamine derivatives as selective acetylcholinesterase (AChE) inhibitor and antioxidant to enhance learning and memory, Biorg. Med. Chem. 25 (4) (2017) 1471–1480.
[51] H. Lineweaver, D. Burk, The determination of enzyme dissociation constants, J. Am. Chem. Soc. 56 (3) (1934) 658–666.
[52] C. Yung-Chi, W.H. Prusoff, Relationship between the inhibition constant (Ki) and the concentration of inhibitor which causes 50 percent inhibition (I50) of an enzymatic reaction, Biochem. Pharmacol. 22 (23) (1973) 3099–3108.
[53] X. Zha, D. Lamba, L. Zhang, Y. Lou, C. Xu, D. Kang, L. Chen, Y. Xu, L. Zhang, A. De Simone, Novel tacrine–benzofuran hybrids as potent multitarget-directed ligands for the treatment of Alzheimer's disease: design, synthesis, biological evaluation, and X-ray crystallography, J. Med. Chem. 59 (1) (2015) 114–131.
[54] M.L. Bolognesi, A. Cavalli, L. Valgimigli, M. Bartolini, M. Rosini, V. Andrisano, M. Recanatini, C. Melchiorre, Multi-target-directed drug design strategy: from a dual binding site acetylcholinesterase inhibitor to a trifunctional compound against Alzheimer's disease, J. Med. Chem. 50 (26) (2007) 6446–6449.
[55] R. Lalonde, The neurobiological basis of spontaneous alternation, Neurosci. Biobehav. Rev. 26 (1) (2002) 91–104.
[56] Z. Bohdanecký, M. Jarvik, Impairment of one-trial passive avoidance learning in mice by scopolamine, scopolamine methylbromide, and physostigmine, Int. J. Neuropharmacol. 6 (3) (1967) 217–222.
[57] M.-R. Lee, B.-S. Yun, S.-Y. Park, S.-Y. Ly, S.-N. Kim, B.-H. Han, C.-K. Sung, Anti-amnesic effect of Chong–Myung–Tang on scopolamine-induced memory impairments in mice, J. Ethnopharmacol. 132 (1) (2010) 70–74.
[58] E. Wills, Mechanisms of lipid peroxide formation in animal tissues, Biochem. J 99 (3) (1966) 667.
[59] A. Kulshreshtha, P. Piplani, Ameliorative effects of amide derivatives of 1, 3, 4-thiadiazoles on scopolamine induced cognitive dysfunction, Eur. J. Med. Chem. 122 (2016) 557–573.
[60] Y. Kono, Generation of superoxide radical during autoxidation of hydroxylamine and an assay for superoxide dismutase, Arch. Biochem. Biophys. 186 (1) (1978) 189–195.
[61] C.J. Weydert, J.J. Cullen, Measurement of superoxide dismutase, catalase and glutathione peroxidase in cultured cells and tissue, Nat. Protoc. 5 (1) (2010) 51.